J. Fluid Mech. (2022), *vol*. 946, A42, doi:10.1017/jfm.2022.632

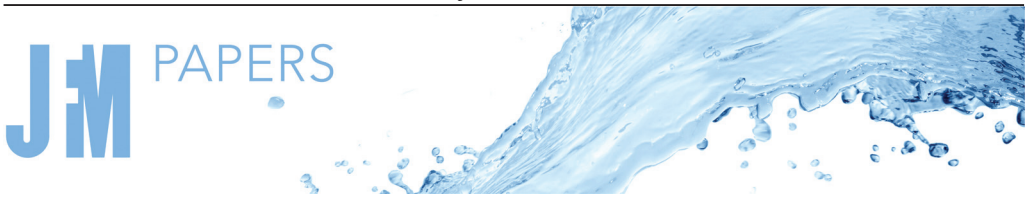

Modelling the transport equation of the scalar structure function

L. Djenidi[1],†, R.A. Antonia[1] and S.L. Tang[2],†

[1]Discipline of Mechanical Engineering, College of Engineering, Science and Environment, University of Newcastle, Newcastle, 2308 NSW, Australia

[2]Center for Turbulence Control, Harbin Institute of Technology, Shenzhen, 518055, PR China

(Received 15 February 2022; revised 16 July 2022; accepted 16 July 2022)

A model for the third-order mixed velocity–scalar structure function $-\overline{(\delta u)(\delta\phi)^2}$ (δa represents the spatial increment of the quantity a; u is the velocity and ϕ is a scalar) is proposed for closing the transport equation of the second-order moment of the scalar increment $\overline{(\delta\phi)^2}$. The closure model is based on a gradient-type hypothesis with an eddy-viscosity model which exploits the analogy between the turbulent kinetic energy and a passive scalar when the Prandtl number, Pr, is equal to 1. The solutions of the closed transport equation agree well with both measurements and numerical simulations, when Pr is not too different from 1. However, the agreement deteriorates when Pr differs significantly from 1. Nevertheless, the calculations capture the effect expected when Pr varies. For example, as Pr increases, a range of scales emerges where $\overline{(\delta\phi)^2}$ remains constant. This emerging scaling range should correspond to the k^{-1} spectral range in the three-dimensional scalar spectrum commonly denoted the viscous–convective range. Also when Pr decreases below 1, the calculations reproduce the emergence of an expected inertial–diffusive range for scales larger than the Kolmogorov length scale.

Key words: turbulence modelling, turbulence theory, isotropic turbulence

1. Introduction

A closure model for the third-order velocity structure function $\overline{(\delta u)^3}$ ($\delta u = u(x) - u(x+r)$, where r is the spatial separation in the longitudinal direction x and the overbar represents ensemble averaging; the time variable is dropped for convenience) was proposed to close

† Email addresses for correspondence: lyazid.djenidi@newcastle.edu.au, Shunlin.tang88@gmail.com

the transport equation for the second-order moment velocity increment $\overline{(\delta u)^2}$, i.e. the the Kármán–Howarth equation (Kármán & Howarth 1938), in homogeneous and isotropic turbulence or HIT (Djenidi & Antonia 2021). The model was shown to yield good agreement with experiments and direct numerical simulations (Djenidi & Antonia 2022).

In the present study we extend this model to the third-order mixed velocity–scalar structure function $-\overline{(\delta u)(\delta\phi)^2}$ in order to solve the transport equation for the scalar structure function for HIT (ϕ is a scalar quantity). Such an equation can be written in the following form (e.g. Danaila *et al.* 1999):

$$-\overline{(\delta u)(\delta\phi)^2} + 2\alpha\frac{\partial\overline{(\delta\phi)^2}}{\partial r} - \frac{1}{r^2}\int_0^r s^2\frac{\partial\overline{(\delta\phi)^2}}{\partial t}\,\mathrm{d}s = \frac{4}{3}\overline{\epsilon_\phi}r. \tag{1.1}$$

The quantity $\overline{(\delta\phi)^2} = \overline{(\phi(x)-\phi(x+r))^2}$ (which we denote S_{ϕ^2} for convenience; also, since $\overline{(\delta\phi)^2}$ is a function of r one should perhaps write $\overline{(\delta_r\phi)^2}$ or S_{r,ϕ^2}; however, we drop the subscript r to avoid cumbersome notation) is the second-order moment of the scalar increment $\delta\phi$. On the left-hand side of (1.1), the first term is the unknown third-order mixed velocity–scalar structure function, the second term is the molecular diffusion and the third term represents the contributions associated with the large-scale motion. This latter term is absent from the well-known Yaglom equation as Yaglom (1949) assumed that $\overline{(\delta\phi)^2}$ is independent of time. On the right-hand side of (1.1), $\overline{\epsilon_\phi} = \alpha\overline{(\partial\phi/\partial x_i)^2}$ is the scalar variance dissipation rate, where α is the diffusivity of ϕ; if the scalar quantity is twice the turbulent kinetic energy ($q^2 = 2k$), then $\overline{\epsilon_q} = \bar{\epsilon} = \nu\overline{(\partial u_i/\partial x_k)^2}$. While (1.1) was initially written for the second-order moment of the temperature increments, it is also valid for any (passive) scalar quantity.

Unlike its spectral counterpart (e.g. Yeh & Atta 1973; Monin & Yaglom 1975), the term $-\overline{(\delta u)(\delta\phi)^2}$ has received less attention in terms of modelling. Danaila, Antonia & Burattini (2012) modelled that term as $(r^2\,\mathrm{d}S_{\phi^2}/\mathrm{d}r)/\tau$, where τ is a characteristic time. Although the authors did not use the model to actually solve (1.1), they nevertheless showed, using experimental data of grid turbulence, that $(r^2\,\mathrm{d}S_{\phi^2}/\mathrm{d}r)/\tau)$ captures the behaviour of $-\overline{(\delta u)(\delta\phi)^2}$ (temperature was used as the passive scalar) reasonably well. There is so far no reported attempt at solving (1.1). Most of the numerical studies on the passive scalar in HIT are carried out via direct numerical simulations (DNSs) or the eddy damped quasi-normal Markovian (EDQNM) approach. The former solve the Navier–Stokes equations coupled with the scalar equation (e.g. Bogucki, Domaradzki & Yeung 1997; Antonia & Orlandi 2002; Yeung, Xu & Sreenivasan 2002; Watanabe & Gotoh 2004; Yeung & Sreenivasan 2014; Gotoh & Watanabe 2015; Shete & de Bruyn Kops 2020; Buaria *et al.* 2021*a*). Unfortunately DNSs are limited to relatively low/moderate Reynolds numbers and Prandtl (or Schmidt) numbers ($Pr = \nu/\alpha$) due to the limitations of computing power as high-Reynolds-number and high-Prandtl-number simulations require very high resolution (see references cited above). The EDQNM approach solves the evolution equations of the kinetic energy and scalar variance spectra (e.g. Briard & Gomez 2017*a*,*b*), where the spectral energy and scalar transfer terms are modelled and can achieve high Reynolds and Prandtl numbers (e.g. Briard & Gomez 2016).

Therefore, the present study is a first attempt at solving (1.1) using a model for $-\overline{(\delta u)(\delta\phi)^2}$. The derivation of the this model is described in § 2. In § 3, a self-similarity analysis is carried out to determine appropriate scaling variables to be used for normalising the solutions to (1.1). Results of solutions to the modelled equation (1.1) for $Pr = 0.7$ and

1 are compared with both DNS and experimental data in § 4 while exploratory predictions at various Reynolds and Prandtl numbers are carried out in § 5. Concluding remarks are provided in § 6.

2. The closure model

One can interpret $(\delta u)(\delta\phi)^2$ as the transport of $(\delta\phi)^2$ by δu. We can then follow Djenidi & Antonia (2020, 2021) and seek to model $S_{u\phi^2} = -\overline{(\delta u)(\delta\phi)^2}$ in the form of a gradient type. We thus model $S_{u\phi^2}$ using a gradient-type hypothesis with an eddy-viscosity model; the model expression for $S_{u\phi^2}$ has the following form:

$$S_{u\phi^2} = \nu_{S_{u\phi^2}} \frac{\partial S_\phi}{\partial r}, \tag{2.1}$$

where $\nu_{S_{u\phi^2}}$ is an eddy viscosity, for which an analytical expression is sought. Djenidi & Antonia (2020, 2021) used the form (2.1) to close the transport equation for $S_{u^2} = \overline{(\delta u)^2}$ and proposed an expression for $\nu_{S_{u^2}}$ based on dimensional arguments. They wrote

$$\nu_{S_{u^2}} \sim u_r l_r, \tag{2.2}$$

where u_r and l_r are velocity and length scales characterising the motion at a scale r. They assumed $u_r \sim (S_u^2)^{1/2}$ and proposed to use $l_r \sim u_r^3/\bar{\epsilon} \sim (S_{u^2})^{3/2}/\bar{\epsilon}$, which leads to

$$\nu_{S_{u^2}} = C_{S_{u^2}} \frac{(S_{u^2})^2}{\bar{\epsilon}}, \tag{2.3}$$

and obtained

$$S_{u^3} = C_{S_{u^2}} \frac{(S_{u^2})^2}{\bar{\epsilon}} \frac{\partial S_{u^2}}{\partial r}, \tag{2.4}$$

where $C_{S_{u^2}}$ is a constant to be determined. The authors showed that this model is unaffected by the intermittency of ϵ. This is consistent with the fact that S_{u^3} is expected not to be affected by such a phenomenon. The transport equation (1.1) is similar for the turbulent kinetic energy, q^2, and any other variance of a passive scalar, ϕ^2, when $Pr = 1$, which suggests an analogy between q^2 and ϕ^2 (Fulachier & Antonia 1984; Abe, Antonia & Kawamura 2009; Antonia, Abe & Kawamura 2009). Using this analogy when $Pr = 1$, we simply adopt the approach of Djenidi & Antonia (2020, 2021) and write (2.1) as follows:

$$S_{u\phi^2} = C_{S_{u\phi^2}} \frac{(S_{q^2})^2}{\bar{\epsilon}} \frac{\partial S_{\phi^2}}{\partial r}, \tag{2.5}$$

where we use $u_r \sim (S_{q^2})^{1/2}$; also note that $\bar{\epsilon} = \bar{\epsilon}_q$. Let us first consider the case where there is a range of scales ($\eta \ll r \ll L$, i.e. the inertial range) over which both the viscous dissipation term and large-scale term (the second and third terms on the left-hand side of

(1.1)) can be neglected. We are then left with

$$C_{S_{u\phi^2}}\frac{(S_{q^2})^2}{\bar{\epsilon}}\frac{\partial S_{\phi^2}}{\partial r}=\frac{4}{3}\bar{\epsilon}_\phi r. \tag{2.6}$$

If $\phi = q$ we then have

$$C_{S_{uq^2}}\frac{(S_{q^2})^2}{\bar{\epsilon}}\frac{\partial S_{q^2}}{\partial r}=\frac{4}{3}\bar{\epsilon} r. \tag{2.7}$$

Integrating and rearranging terms leads to

$$S_{q^2}=C_q(\bar{\epsilon}r)^{2/3}, \tag{2.8}$$

with $C_q = (2/C_{S_{uq^2}})^{1/3}$. Antonia *et al.* (1996) showed that $C_q = (11/3)C_K$, where C_K is the Kolmogorov constant in $S_{u^2} = C_K(\bar{\epsilon}r)^{2/3}$. Now taking $\phi = \theta$ (say the temperature fluctuation) leads to

$$C_{S_{u\theta^2}}\frac{(S_{q^2})^2}{\bar{\epsilon}}\frac{\partial S_{\theta^2}}{\partial r}=\frac{4}{3}\bar{\epsilon}_\theta r. \tag{2.9}$$

Assuming we are in the range of scales over which (2.8) is valid and the second and third terms on the left-hand side of (1.1) are also negligible when $\phi = \theta$, we then have

$$C_{S_{u\theta^2}}\frac{C_q^2(\bar{\epsilon}r)^{4/3}}{\bar{\epsilon}}\frac{\partial S_{\theta^2}}{\partial r}=\frac{4}{3}\bar{\epsilon}_\theta r. \tag{2.10}$$

Integrating this expression leads to

$$S_{\theta^2}=C_\theta\bar{\epsilon}_\theta\bar{\epsilon}^{-1/3}r^{2/3}, \tag{2.11}$$

where $C_\theta = 2/(C_q^2 C_{S_{u\theta^2}})$ is a constant to be determined. Antonia *et al.* (1996) estimated that $C_\theta = C_q R$, where $R = (\overline{\theta^2}/\bar{\epsilon}_\phi)/(\overline{q^2}/\bar{\epsilon})$ is the dissipation time-scale ratio. Note that the constants C_K and C_θ are not to be confused with their spectral counterparts (Sreenivasan 1995, 1996). Below we test the model and compare the results against available data. However, we need first to determine appropriate scaling parameters. This is addressed in § 3.

3. Scaling variables

Before we solve (1.1) where the closure model (2.5) is introduced, we first seek self-preservation (SP) solutions to (1.1) to allow us to determine appropriate scaling variables. We seek solutions in the following form:

$$S_{\phi^2}=\phi_*^2(t)f_\phi(r_\phi^*),\quad S_{u^2}=u_*^2(t)f_u(r_\phi^*),\quad S_{u\phi^2}=B_*(t)g_\phi(r_\phi^*), \tag{3.1a–c}$$

with $r_\phi^* = r/l_\phi(t)$, and $l_\phi(t)$, $u_*(t)$ and $\phi_*(t)$ are the length, velocity and scalar scaling functions to be determined, $B_*(t)$ is a mixed scaling and f_ϕ and f_u are dimensionless functions. For convenience, we hereafter drop the variable t. Let us introduce the mixed skewness increment $S(r)$ ($\equiv S_{u\phi^2}/[S_{u^2}^{1/2}S_{\phi^2}]$). If SP is satisfied, $S(r)$ has also the SP form

$S(r) = c_\phi(t) H_\phi(r^*_\phi)$. We thus can take $B_* = u_* \phi_*^2$. Substituting the form (3.1*a–c*) into (1.1) leads to the following equation if SP is satisfied:

$$-Re_{l_\phi} g_\phi(r^*_\phi) + 2f'_\phi(r^*_\phi) - \frac{l_\phi^2}{\alpha \phi_*^2}\frac{\partial \phi_*^2}{\partial t}\frac{\Gamma_{1,\phi}}{r_\phi^{*2}} + \frac{l_\phi}{\alpha}\frac{\partial l_\phi}{\partial t}\frac{\Gamma_{2,\phi}}{r_\phi^{*2}} = \frac{4}{3}\frac{\overline{\epsilon_\phi} l_\phi^2}{\alpha \phi_*^2} r^*_\phi, \tag{3.2}$$

and the constraints on the various scaling variables

$$C_1 = Re_{l_\phi}, \tag{3.3}$$

$$C_2 = 2, \tag{3.4}$$

$$C_3 = \frac{l_\phi^2}{\alpha \phi_*^2}\frac{\partial \phi_*^2}{\partial t}, \tag{3.5}$$

$$C_4 = \frac{l_\phi}{\alpha}\frac{\partial l_\phi}{\partial t}, \tag{3.6}$$

$$C_5 = \frac{\overline{\epsilon_\phi} l_\phi^2}{\alpha \phi_*^2} \tag{3.7}$$

(a prime denotes a derivative with respect to r^*_ϕ), where $Re_{l_\phi} = u_* l_\phi / \alpha$ is a scaling Reynolds number or Péclet number and

$$\Gamma_{1,\phi} = \int_0^{r^*_\phi} s_\phi^{*2} f_\phi \, \mathrm{d}s_\phi^{*2}, \quad \Gamma_{2,\phi} = \int_0^{r^*_\phi} s_\phi^{*3} f'_\phi \, \mathrm{d}s_\phi^{*2}. \tag{3.8a,b}$$

Since C_2 is a constant, then C_1, C_3, C_4 and C_5 are also constants and thus time-independent. Combining (3.4) and (3.7) (we multiplied the numerator and denominator of the latter by u_*^2) and using the definition of Re_{l_ϕ} yields

$$l_\phi = (\sqrt{C_5} C_1)^{1/2} \left(\frac{\alpha^3}{\overline{\epsilon_\phi}}\right)^{1/4} \left(\frac{\phi_*}{u_*}\right)^{1/2}. \tag{3.9}$$

Now, substituting (3.9) in (3.7) leads to

$$\phi_* = \left(\frac{C_1}{\sqrt{C_5}}\right) (\alpha \overline{\epsilon_\phi})^{1/2} \frac{1}{u_*}. \tag{3.10}$$

Let us first consider the turbulent kinetic energy as the passive scalar. Thus, $S_{\phi^2} = S_{q^2}$ and $\alpha = \nu$, $\phi_* = u_*$ and $\overline{\epsilon_\phi} = \bar{\epsilon}$ (the mean turbulent kinetic energy dissipation rate), and recognising that $\eta = (\nu^3/\bar{\epsilon})^{1/4}$ and $v_K = (\nu \bar{\epsilon})^{1/4}$ (the Kolmogorov length and velocity, respectively), we can write

$$l_q = C_{l_q} \eta, \quad u_* = C_{u_*} v_K. \tag{3.11a,b}$$

If we now consider that the passive scalar is the temperature, we have $S_{\phi^2} = S_{\theta^2}$ and denote α a thermal diffusivity, for example. This leads to

$$l_\theta = C_{l_\theta} \eta_\theta \left(\frac{\theta_*}{u_*}\right)^{1/2}, \quad \theta_* = C_{\theta_*} v_\theta^2 \frac{1}{u_*}, \tag{3.12a,b}$$

where we define for convenience $\eta_\theta = (\alpha^3/\overline{\epsilon_\theta})^{1/4}$ and $v_\theta = (\alpha \overline{\epsilon_\theta})^{1/4}$.

Substituting the second expression of (3.12*a*,*b*) into the first expression and taking $u_* = v_K$, we obtain

$$l_\theta = C_{l_\theta} C_{\theta_*}^{1/2} \frac{1}{Pr^{1/4} R_\epsilon^{1/4}} \eta_\theta = C_{l_\theta} C_{\theta_*}^{1/2} \frac{1}{Pr^{1/4}} \tilde{\eta}_\theta, \tag{3.13}$$

where $R_\epsilon = (\bar{\epsilon}/\overline{\epsilon_\theta})$, $\tilde{\eta}_\theta = (\alpha^3/\bar{\epsilon})^{1/4}$ and $Pr = \nu/\alpha$ is the Prandtl number. Hereafter and for convenience we use the notation Pr independently of whether the scalar is the temperature or any other quantity different from q. Note that we can also write (3.13) as

$$l_\theta = C_{l_\theta} C_{\theta_*}^{1/2} \frac{1}{Pr^{1/2}} \left(\frac{\alpha^2 \nu}{\bar{\epsilon}} \right)^{1/4} \tag{3.14}$$

or

$$l_\theta = C_{l_\theta} C_{\theta_*}^{1/2} \frac{1}{Pr} \eta. \tag{3.15}$$

Now, we have for θ_*

$$\theta_* = C_{\theta_*} \frac{1}{v_K} v_\theta^2 = C_{\theta_*} \frac{1}{Pr^{1/4} R_\epsilon^{1/4}} v_\theta. \tag{3.16}$$

The derivation of the scaling variables (3.11*a*,*b*) from the equations of motion has been already shown and discussed elsewhere (Djenidi, Antonia & Danaila 2017). Several expressions for l_θ, based on dimensional arguments, have been formulated in the literature. For example, Oboukhov (1949) and Corrsin (1951) obtained

$$l_C = \left(\frac{\alpha^3}{\bar{\epsilon}} \right)^{1/4}, \tag{3.17}$$

which is simply $\tilde{\eta}_\theta$, while Batchelor (1959) obtained

$$l_B = \left(\frac{\alpha^2 \nu}{\bar{\epsilon}} \right)^{1/4}. \tag{3.18}$$

These length scales are related as follows:

$$l_C = \frac{1}{Pr^{1/4}} l_B. \tag{3.19}$$

These two length scales are related to η as follows:

$$l_C = \frac{1}{Pr^{3/4}} \eta, \tag{3.20}$$

$$l_B = \frac{1}{Pr^{1/2}} \eta. \tag{3.21}$$

Finally we have the following relation:

$$l_\theta = C_{l_\theta} C_{\theta_*}^{1/2} \frac{1}{Pr^{1/4}} l_C = C_{l_\theta} C_{\theta_*}^{1/2} \frac{1}{Pr^{1/2}} l_B, \tag{3.22}$$

which shows how the present length scale, l_θ, issued from the SP analysis, relates to the empirical length scales of Corrsin and Batchelor, L_C and L_B, respectively.

4. Numerical solutions

Let us for convenience denote hereafter the integral term in (1.1) as Z_ϕ. Using a linear forcing in the context of the Kármán–Howarth equation (Kármán & Howarth 1938) expressed in terms of S_{u^2}, Lundgren (2003) showed that for stationary HIT the integral term corresponding to that in (1.1) can be replaced by a term, Z_u, of the following expression:

$$Z_u = \frac{2\bar{\epsilon}}{u'^2}\frac{1}{r^4}\int_0^r s^4 S_{u^2}\,\mathrm{d}s, \tag{4.1}$$

and suggested that this forcing is equivalent to a uniform spectral forcing at all wavenumbers and can allow comparison with decaying HIT. By analogy to (4.1), and since we consider stationary HIT, we express $Z_\phi(r)$ as follows:

$$Z_\phi = \frac{2\bar{\epsilon}_\phi}{\phi'^2}\frac{1}{r^2}\int_0^r s^2 S_{\phi^2}\,\mathrm{d}s, \tag{4.2}$$

which gives the correct asymptotic limit $Z_\phi = \frac{4}{3}\overline{\epsilon_\phi} r$ when $r/\eta \to \infty$. Substituting (2.5) and (4.2) in (1.1) we can solve the resulting equation in the following simple manner:

$$S_{\phi^2}(r+\Delta r) = S_{\phi^2}(r) + \frac{\{\frac{4}{3}\overline{\epsilon}_\phi r - Z_\phi\}\Delta r}{2\alpha + C_{S_{u\phi^2}}[S_{q^2}(r)]^2/\bar{\epsilon}}, \tag{4.3}$$

where the calculations start by evaluating the right-hand side of (4.3) at $r = \eta + \Delta r$ with the boundary condition $S_{\phi^2} = (1/3\alpha)\overline{\epsilon_\phi} r^2$ at $r = \eta$, which is the correct solution of (1.1) in the viscous–diffusive range. The process is then repeated by increment of Δr. Note that (4.3) requires knowledge of S_{q^2} when ϕ^2 is any passive scalar variance different from the turbulent kinetic energy. Consequently, solutions of S_{q^2} using (4.3) are obtained first before (4.3) is used again to obtain solutions of S_{ϕ^2}. In all calculations we follow Antonia *et al.* (1996) and use $C_q = (11/3)C_K = 7.3$, where we assume $C_K = 2$. For C_θ we use the value matching that corresponding to the data we used for comparison; that value varies from 2.8 to 4. A definitive value is yet to be determined, although it is thought that a value of 3.2 corresponds to the equivalent spectral constant which has a value of 0.4 (e.g. Monin & Yaglom 1975). To perform the calculation we use the values of $\bar{\epsilon}$, $\overline{\epsilon_\theta}$, q^2 and θ^2 reported in the references we have used to compare to. This ensures similar values of the dissipation time-scale ratio R between our calculations and those of the references. Note that for clarity we take $\phi = q$ when the scalar is the turbulent kinetic energy and $\phi = \theta$ for any other passive scalar.

We first test the calculations against large Taylor microscale Reynolds number ($Re_\lambda = 2 \times 10^4$, where λ is the Taylor microscale) EDQNM simulations of decaying HIT with $Pr = 1$ (Briard & Gomez 2017*a*). The results are reported in figure 1 which shows a comparison between the calculated distributions of S_{ϕ^2} and $S_{u\phi^2}$ with their EDQNM counterparts. There is generally good agreement between the present calculations and the EDQNM simulations. It should be pointed out that $S_{u\phi^2}$ is calculated using (2.5) once the distribution of S_{ϕ^2} is obtained with (4.3). Notice the relatively good agreement for S_{ϕ^2} at small separations, i.e. $0 \leq r/\eta \leq 10$. This is remarkable considering that the model (2.5) is not in principle adequate for the region outside the scaling range, as indeed observed for $S_{u\phi^2}$. The reason why the calculated distribution of S_{ϕ^2} is not significantly affected by the relatively poor performance of the model $S_{u\phi^2}$ at small separations relates to the fact that $S_{u\phi^2}$ approaches zero at a faster rate than the viscous term (second term on the

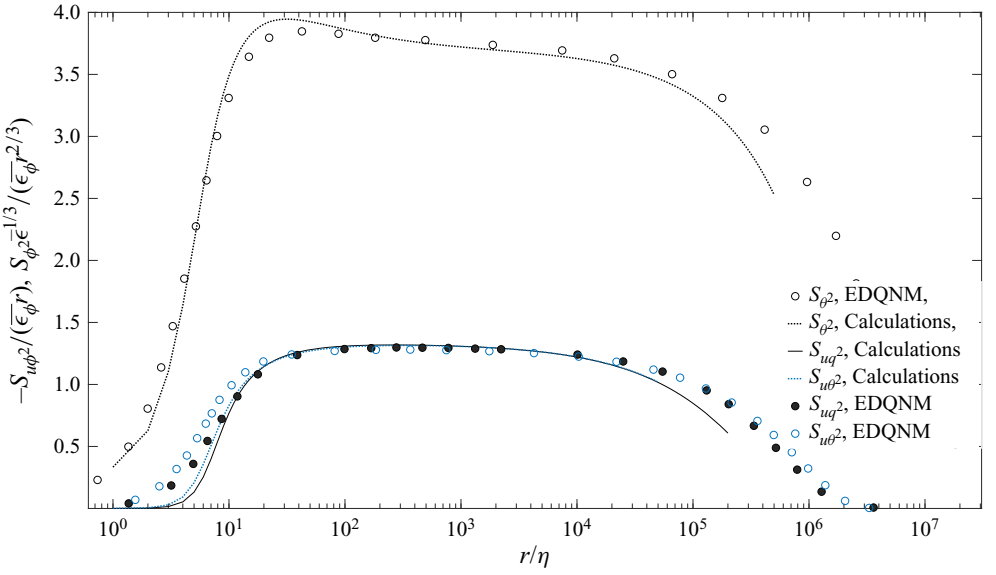

Figure 1. Distributions of the second-order scalar structure function S_{ϕ^2} and mixed structure function $S_{u\phi^2}$ for $Pr = 1$ and $Re_\lambda = 2 \times 10^4$. Symbols: EDQNM decaying turbulence (Briard & Gomez 2017*a*); lines: present calculations; S_{ϕ^2} is calculated using (4.3) and $S_{u\phi^2}$ is calculated using (2.5).

left-hand side of (1.1)). Indeed, $S_{u\phi^2} \sim r^3$ while $\partial S_{\phi^2}/\partial r \sim r$ as $r \to 0$. The model (2.5) behaves like r^5 as $r \to 0$, thus leaving the solutions for S_{ϕ^2} practically unaffected. For large separations the model also performs imperfectly. But once again this is not critical since $S_{u\phi^2}$ approaches zero and the integral term in (1.1) dominates the budget. One possible reason for the small difference between the present results and the EDQNM results at large separations may relate to the fact that the EDQNM does not use non-local transfers to solve Lin's equation. Altogether, figure 1 shows that (2.5) provides an adequate closure for (1.1). This is supported by figures 2 and 3 which show comparisons between the present calculations and both experimental data (grid turbulence, Mydlarski & Warhaft (1998); wake, Antonia *et al.* (1996); jet, Burattini, Antonia & Danaila (2005)) and DNS data of forced HIT (Watanabe & Gotoh 2004); $Pr = 0.71$ and 1 for the experiments and DNSs, respectively. The results indicate that the linear forcing represented by (4.2) is adequate for the scalar field and that it reproduces adequately the large-scale motion contributions in both decaying and forced turbulence. This is further reinforced by comparing the present calculations with the DNS results for HIT fed by a mean scalar gradient at $Pr = 1$ (Gauding, Danaila & Varea 2017) as seen in figure 4. We used values of $\bar{\epsilon}$, $\overline{\epsilon_\theta}$, q^2 and θ^2 reported in Gauding *et al.* (2017); R varies from about 0.48 to 0.423 when Re_λ varies from 88 to 529. There is very good agreement between the DNS results and the calculations.

5. Exploratory predictions based on the modelled form of (1.1)

5.1. *Effect of Pr*

In the previous section we showed that (2.5) is an adequate closure model for (1.1) at moderately high Reynolds number and at least when Pr is not too different from 1. However, since the present model (2.5) uses an analogy between the turbulent kinetic

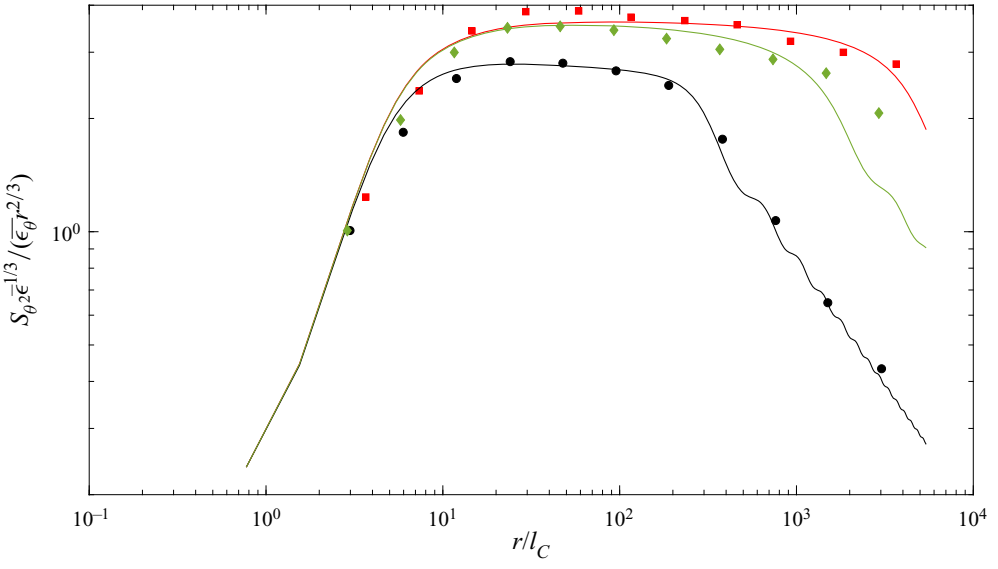

Figure 2. Distributions of the second-order temperature structure function S_{ϕ^2} ($\phi = \theta$) for $Pr = 0.71$. Symbols: decaying grid turbulence (Mydlarski & Warhaft 1998); lines: present calculations; S_{ϕ^2} is calculated using (4.3).

energy and a scalar variance field when $Pr = 1$ it is worth assessing its performance when this analogy is not valid, i.e. when Pr differs markedly from 1.

Figure 5 compares the present calculations at $Pr = 1$, 4, 8, 16, 32 and 64 and $Re_\lambda = 38$ with the DNS data of Yeung *et al.* (2002) for HIT where the scalar field is forced via a uniform mean scalar gradient at similar Pr and Re_λ. We used the values of $\bar{\epsilon}$, $\overline{\epsilon_\theta}$, q^2 and θ^2 reported in table II of Borgas *et al.* (2004) which leads to the dissipation time-scale ratio R ranging from 0.6 to 1.3 when Pr varies from 1 to 64, respectively. While the present calculations reproduce the fanning effect of increasing Pr observed for the DNS data, they overpredict S_{ϕ^2} in the region between the small and large scales. This would suggest that the dependence of Pr (or of R) should somehow be incorporated in the model (2.5).

In figure 6 we compare the present calculations at $Pr = 1$, 1/8, 1/128, 1/512 and 1/2048 and $Re_\lambda = 240$ with the DNS data of Yeung *et al.* (2002) (for $Pr = 1$ and 1/8) and Yeung & Sreenivasan (2014) (for $Pr = 1/128$, 1/512 and 1/2048) at the same Reynolds number; these distributions are computed via the relation

$$S_{\phi^2}(r) = 2\int_0^\infty E_\phi(k)\left(1 - \frac{\sin kr}{kr}\right)\mathrm{d}k, \tag{5.1}$$

where $E_\phi(k)$ is the scalar variance spectrum. We used the values of $\bar{\epsilon}$, $\overline{\epsilon_\theta}$, q^2 and θ^2 reported in tables I and III of Yeung & Sreenivasan (2014); R varies from 0.43 to 0.11 when Pr decreases from 1 to 1/2048. While the present calculation captures the effect of decreasing Pr, the agreement between the calculations and DNS deteriorates as Pr decreases. The reason for this deterioration is yet to be determined. One can speculate that perhaps the model (2.5), which is based on the analogy between q^2 and ϕ^2 when $Pr = 1$, fails to capture for the effect of decreasing Pr. Also, we should recall that local isotropy is assumed in (1.1). Since the scalar anisotropy increases when Pr decreases below 1, as reflected in the increase of the scalar derivative skewness (Buaria *et al.* 2021*b*), it is possible that the deterioration of the results illustrates the gradual departure from local

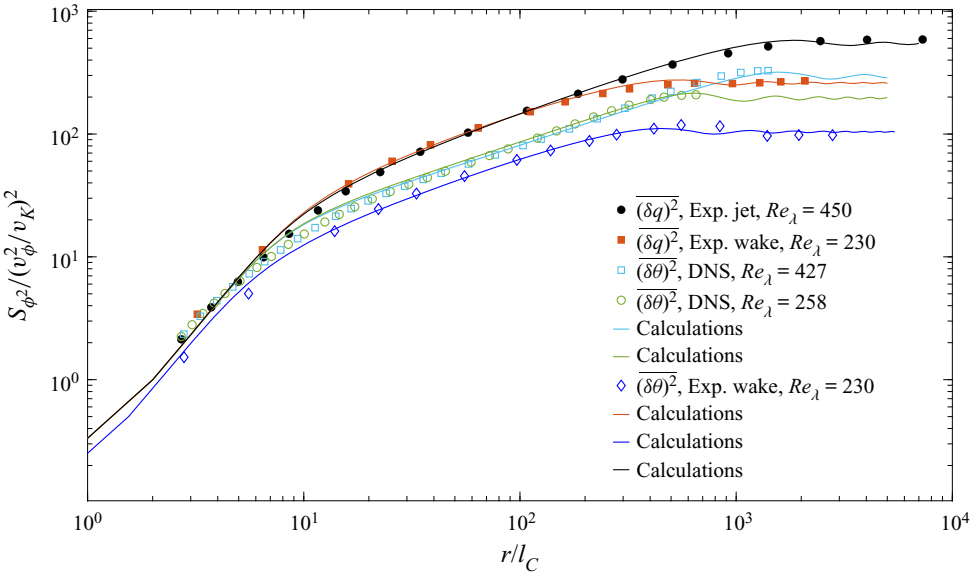

Figure 3. Distributions of the second-order structure function S_{ϕ^2} as a function of r/l_C. Symbols: measurements ($Pr = 0.7$) on centrelines of a cylinder wake at $Re_\lambda = 230$ (Antonia *et al.* 1996) and round jet flow at $Re_\lambda = 450$ (Burattini *et al.* 2005) and DNS of HIT, $Re_\lambda = 258$ and 427, $Pr = 1$ (Watanabe & Gotoh 2004); lines: calculations; S_{ϕ^2} is calculated using (4.3).

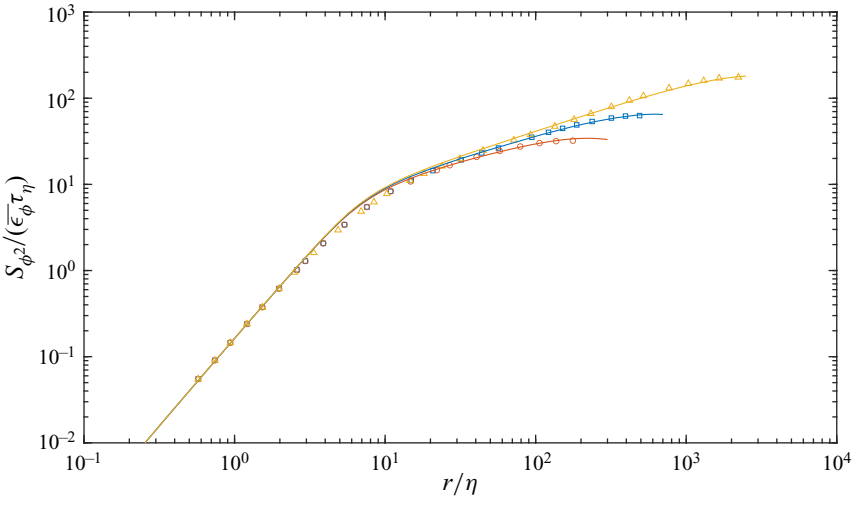

Figure 4. Distributions of the second-order structure function S_{ϕ^2} as a function of r/l_C. Symbols: DNS of HIT with a scalar mean gradient, $Re_\lambda = 88$ (circles), 184 (squares) and 529 (triangles), $Pr = 1$ (Gauding *et al.* 2017); $\tau_\eta = (\nu/\overline{\epsilon})^{1/2}$. Lines: calculations; S_{ϕ^2} is calculated using (4.3).

isotropy, making the present prediction less adequate as Pr decreases. Finally, it is also possible that discrepancies between the present calculation and DNS when Pr differs from 1 can be due to the presence of a mean scalar gradient in the DNS. Indeed, the forcing (4.2) does not reflect he axisymmetric configuration resulting from a mean scalar gradient.

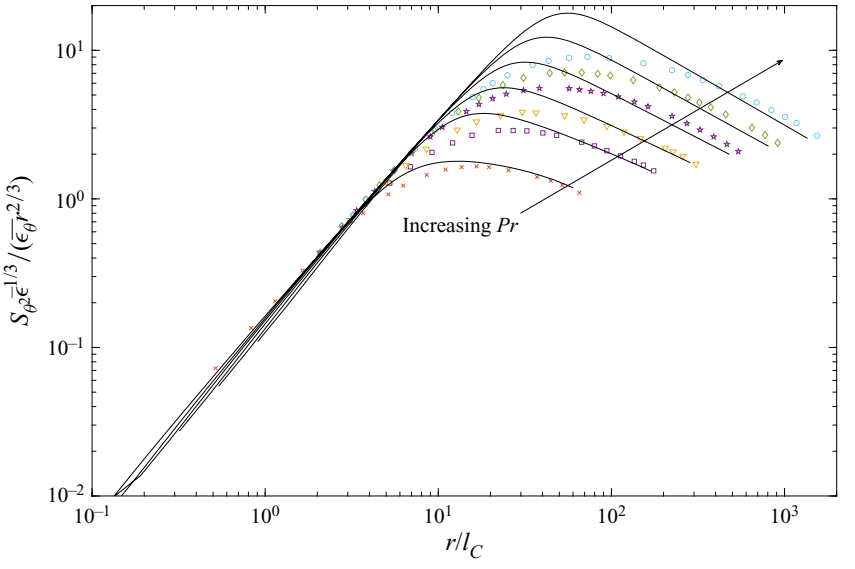

Figure 5. Distributions of the second-order temperature structure function S_{ϕ^2} ($\phi = \theta$) for $Pr = 1$, 4, 8, 16, 32 and 64 and $Re_\lambda = 38$. Symbols: DNS of HIT with uniform mean scalar gradient (Yeung *et al.* 2002). Lines: present calculations.

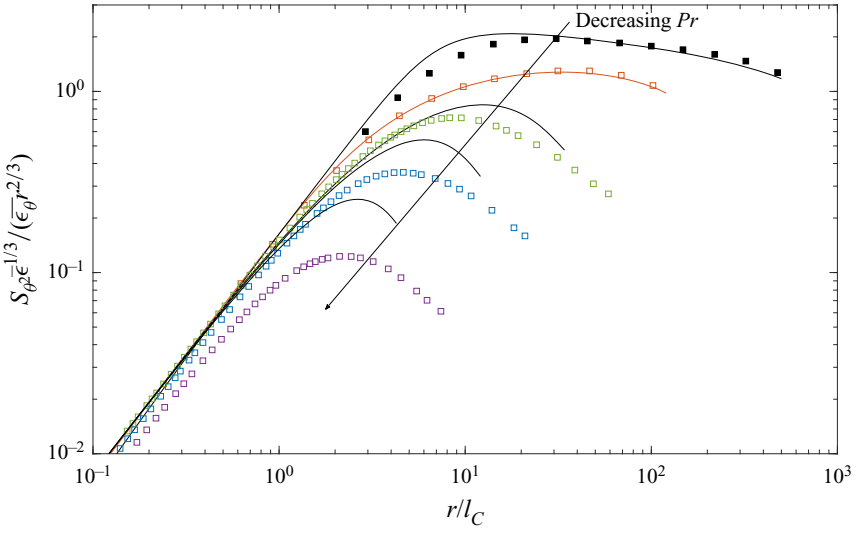

Figure 6. Distributions of the second-order temperature structure function S_{ϕ^2} ($\phi = \theta$) for $Pr = 1/8$, 1, 1/128, 1/512 and 1/2048 and $Re_\lambda = 240$. Symbols: DNS of HIT with uniform mean scalar gradient (Yeung *et al.* 2002; Yeung & Sreenivasan 2014). Lines: present calculations.

5.2. *Effect of Re_λ when $Pr = 1$*

The value of the dissipation time-scale ratio R ranged from 0.4 to 0.53 in all the experimental, DNS and EDQNM data reported in § 4, where $Pr = 1$. One can then explore the effect of Re_λ when $Pr = 1$ and R is maintained constant. So for this exploratory prediction we retain the values of $\bar{\epsilon}$, $\overline{\epsilon_\theta}$, q^2 and θ^2 reported in Watanabe & Gotoh (2004) for $Re_\lambda = 258$; this is equivalent to maintaining the dissipation time-scale ratio R

constant ($R = 0.53$). Some comments regarding the constancy of R are warranted though. Ristorcelli (2006) showed that R can be expressed as

$$R = 0.5\left(\frac{L_\phi}{L}\right)^{2/3} = \frac{5}{3}Pr\frac{\lambda_\phi^2}{\lambda^2}, \tag{5.2}$$

where $L = k^{3/2}/\bar{\epsilon}$ and $L_\phi = (\bar{\epsilon}^{1/3}\overline{\phi^2}/\bar{\epsilon}_\phi)^{3/2}$ are energy and scalar integral length scales, respectively, and λ_ϕ^2 is the scalar microscale (note that Ristorcelli (2006) defines his dissipation time-scale ratio as $1/R$). Thus, maintaining R constant is equivalent to maintaining the ratio of the energy and scalar injection length scales constant, or if Pr is constant, keeping the ratio of the microscales constant. Interestingly, (L_ϕ/L) reported in Donzis, Sreenivasan & Yeung (2005) is approximately constant for $Pr = 1$ when Re_λ varies from 8 to 390. It is marginally changed when Re_λ varies from 8 to 38. Also table I of Yeung *et al.* (2002) shows that R has the values 1.78, 2.36 and 2.33 for $Re_\lambda = 38$, 140 and 240 when $Pr = 1$. Yeung *et al.* (2004) conclude from their data for $Re_\lambda = 38$ where Pr varies from 64 to 1024 that R decreases slightly. Of course, it is possible that R could change significantly when Re_λ varies over a much larger range than reported for the DNS data. It is nevertheless of interest to assess the behaviour of S_{ϕ^2} with increasing Reynolds number when $Pr = 1$ and R is fixed. Numerical simulations allow such an analysis. For example, Jiang & O'Brien (1991) carried out an analysis with $L_\phi/L = $ const. and varying λ_ϕ/λ. They found no significant change in the mixing rate. However a significant change was observed when they varied L_ϕ/L while λ_ϕ/λ was maintained constant. The results of Gauding *et al.* (2017) as well as those of Donzis *et al.* (2005) (see inset of their figure 2) showing that R does not change significantly with increasing Re_λ provide some justification for maintaining R constant when $Pr = 1$. Finally, one can write

$$R = \frac{\overline{\theta^2}/\bar{\varepsilon}_\theta}{\overline{q^2}/\bar{\varepsilon}} = \frac{\overline{\theta^2}\bar{\varepsilon}}{3\overline{u^2}\bar{\varepsilon}_\theta} = \frac{\dfrac{\bar{\varepsilon}L}{\overline{u^2}^{3/2}}}{\dfrac{3\bar{\varepsilon}_\theta L}{\overline{u^2}^{1/2}\overline{\theta^2}}} = \frac{C_\varepsilon}{3C_{\varepsilon_\theta}}. \tag{5.3}$$

It is well accepted that C_ϵ becomes approximately constant when $Re_\lambda \gtrsim 100$ in HIT (e.g. Donzis *et al.* 2005; Ishihara, Gotoh & Kaneda 2009). Further, figure 1 of Buaria *et al.* (2021*a*) shows that $C_{\epsilon_\theta}$is also approximately constant when the Péclet number ($Pe \equiv Re_\lambda Pr$) becomes larger than about 200 when $Pr = 1$. This supports the assumption of a constant R when $Pr = 1$ and Re_λ is large. This provides some confidence in the present exploratory analysis at fixed Pr and R and varying Reynolds number. The Reynolds number is increased by simply decreasing ν and keeping the other parameters unchanged. The results are reported in figure 7 where we show the distributions of S_{ϕ^2} for all Re_λ and the distribution of S_{q^2} for the largest Re_λ. This latter distribution collapses well with that of S_{ϕ^2} in the region $0 \leq r/\eta \leq 10$. In this region both S_{ϕ^2} and S_{q^2} follow the behaviour $S_{\phi^2}/(v_{\phi^2}^2/v_K)^2) \sim (r/\eta)^2$. This range of scales is commonly denoted as the viscous–diffusive range and the collapse between S_{ϕ^2} and S_{q^2} is expected when $Pr = 1$ (i.e. $\alpha = \nu$). Note that since $S_{\phi^2} = (1/3\alpha)\overline{\epsilon_\phi}r^2$ in this range, the collapse is independent of whether or not $\bar{\epsilon}$ and $\overline{\epsilon_\phi}$ are equal. Beyond this range, the distributions of S_{ϕ^2} and S_{q^2} differ but remain parallel to each other; the difference reflects the difference between $\overline{\epsilon_\phi}$ and $\bar{\epsilon}$; these values are 0.558 and 0.507, respectively (see Watanabe & Gotoh 2004). For the largest Reynolds number three subranges (marked in the figure) are well defined: viscous–diffusive range, inertial–convective range (ICR) and large-scale range. In the first

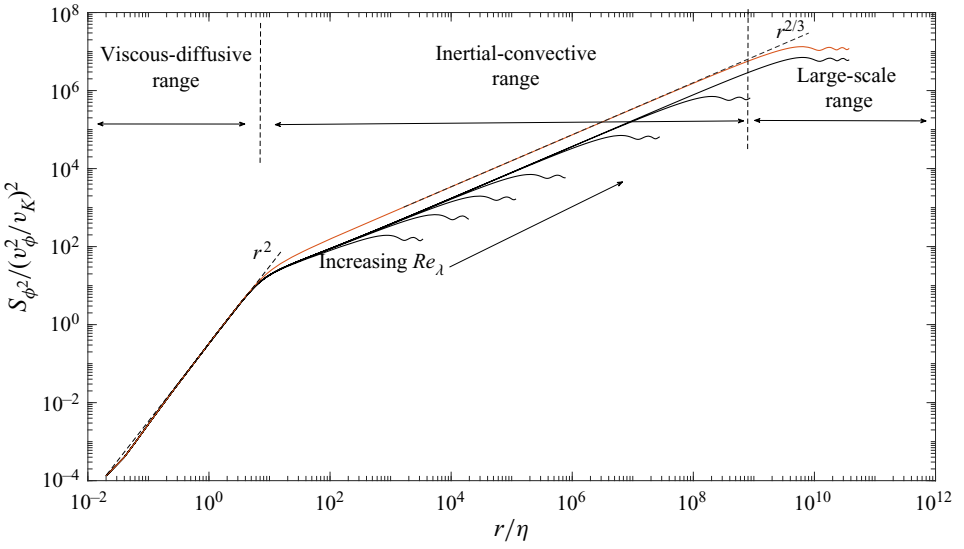

Figure 7. Distributions of the second-order scalar structure function S_{ϕ^2} as a function of r/η for $Pr = 1$, and $Re_\lambda = 258$, 10^3, 3×10^3, 1.15×10^4, 1.15×10^5, 1.15×10^6 and 1.15×10^7. Black lines: S_{θ^2}. Red line: S_{q^2} (only for $Re_\lambda = 1.15 \times 10^7$).

range, as seen above $S_{\phi^2} \sim r^2$. In the second range $S_{\phi^2} \sim r^{2/3}$, while S_{ϕ^2} is constant in the third range. Interestingly, the similarity of the distribution shape between S_{ϕ^2} and S_{q^2} suggests a very good analogy between the turbulent kinetic energy field and any other passive scalar variance field at all scales of motion when $Pr = 1$.

5.3. *Effect of large variations of Pr for fixed Re_λ and R*

We complete these exploratory predictions by looking at the effect of large variations of Pr for $Re_\lambda = 1.15 \times 10^7$. We use this large value of Re_λ to ensure that an ICR is reasonably established, as seen in figure 7, and the effect of the large-scale motion on the small-scale turbulence is minimised. Note that all real viscous flows (with non-zero viscosity) are at finite Reynolds numbers: even Re_λ of the order of 10^{10} or 10^{20} is finite. Infinite Reynolds number can occur only for inviscid flows, where there is no no-slip condition. Accordingly, all flows that are not at infinite Reynolds number are, in principle, never fully free of the effect of the large-scale motion (for convenience denoted finite Reynolds number effect). Nevertheless, in very-large-Reynolds-number turbulent flows where there is a large separation between the small and large scales, one can reasonably expect that the finite Reynolds number effect is minimised, if not neglected, on the small-scale turbulence.

According to (5.2), one can expect a Pr dependence of R. Yeung *et al.* (2002) suggested that in general such a dependence should be incorporated in modelling. Nevertheless, the assumption of constant R is used in engineering turbulence models to avoid solving an equation for $\bar{\epsilon}_\phi$ (Hanjalić 2002). Ristorcelli (2006) argued that turbulence models based on constant R may not be useful in any flow in which the production of the scalar and the velocity field have different time or length scales. Here, we follow Hanjalić (2002) and keep R constant and equal to 0.53, even though the present model (2.5) is developed when Pr is not too different from 1, i.e. when the analogy between the turbulent kinetic energy and any other variance of a passive scalar holds. The results are shown in figure 8

which reports $S_{\phi^2}/\overline{\phi^2}$ as a function of r/η and where Pr decreases from 10^7 to 10^{-7}. When Pr increases from 1 to 10^7, one observes the emergence of a plateau, hereafter denoted the viscous–convective range (VCR). Assuming that S_{ϕ^2} in the VCR depends on $\overline{\epsilon_\phi}$, $(\bar{\epsilon}/\nu)^{1/2}$ and r, Antonia & Orlandi (2002) used dimensional analysis to show that S_{ϕ^2} is independent of r and proportional to $\overline{\epsilon_\phi}/(\bar{\epsilon}/\nu)^{1/2}$. This is consistent with the present results. The emergence of a VCR is consistent with the behaviour of the three-dimensional scalar spectrum as depicted in figure 8.11 of Tennekes & Lumley (1972) and figure 2(a) of Briard & Gomez (2016). In this range $E(k) \sim k^{-1}$ according to Batchelor (1959). When $Pr \geq 10^2$, one can identify five subranges (marked in the figure for $Pr = 10^7$) in the distribution of S_{ϕ^2}: viscous–diffusive range, VCR, transition range, ICR and large-scale range. The lower limit of the VCR decreases below η as Pr increases; the large variation of Pr allows a clear assessment of the behaviour of this lower limit. Also, the upper limit of this range extends well beyond η at variance with the classical expectation that this limit is located below η (Batchelor 1959). The k^{-1} spectral range is commonly defined as $\eta^{-1} < k < l_B^{-1}$. The present results are consistent with those of Bogucki *et al.* (1997) who observed that the k^{-1} spectral range extends to $k < \eta^{-1}$; see also Yeung *et al.* (2002) for a similar observation. Antonia & Orlandi (2002) commented on the possibility that the onset of the VCR occurs when r is greater than η. The VCR is followed by a transition range which marks the gradual diminishing effect of ν with increasing r/η and leading to the ICR. When Pr decreases from 1 to 10^{-7}, a range of scales, which is commonly denoted as the inertial–diffusive range, emerges and increases to the detriment of the ICR. Notice that the magnitude of S_{ϕ^2} decreases as Pr decreases, reflecting an increase of the scalar diffusivity α, and thus a stronger diffusion of the scalar ϕ. The inset of figure 8 shows the EDQNM calculations of S_{ϕ^2} in decaying HIT for $Re_\lambda = 1000$ ($Pr = 10^5$, 10^3 and 1) and 20 000 ($Pr = 10^{-3}$ and 10^{-5}) (Briard & Gomez 2015, 2016) and HIT in the presence of uniform mean scalar gradient for $Re_\lambda = 140$, $Pr = 1, 32$, and 512 (Buaria *et al.* 2021*b*). We use the EDQNM and DNS spectra (the spectra of Buaria *et al.* (2021*b*) are from their supplementary material) to calculate S_{ϕ^2} according to (5.1). The EDQNM data suggest the emergence of a plateau as Pr increases beyond 1 while the inertial–diffusive range increases to the detriment of the ICR as Pr decreases below 1. The DNS data also indicate a trend for the emergence of a plateau with increasing Pr. This trend is less marked than in the EDQNM data perhaps due to the relatively lower value of the Reynolds number.

Some comments with regard to the present calculations are warranted. It is quite remarkable that while the model (2.5) does not explicitly account for the effect of Pr and R is kept constant, the calculations do capture the expected effect of an increasing Pr, that is, the emergence of a VCR observed in the EDQNM data and to some extent in the DNS data. Nevertheless, the present results shown in figure 8, need to be considered with caution. Indeed, it is most likely that R will vary with Pr. One can perhaps expect that the variation of R should have an impact on the results if such a variation is explicitly accounted for in the model. For example, the emergence of the plateau in S_{ϕ^2} could be more gradual and less 'abrupt' than for the present prediction and more in line with the trend of the EDQNM and DNS data. A possible first attempt, which is beyond the scope of the present study, to account for the variation of R with Pr can be carried out using the relation $R = C_\epsilon/3C_{\epsilon\theta}$, where C_ϵ is approximately constant ($\simeq 0.5$) when $Re_\lambda \gtrsim 100$ in HIT (Donzis *et al.* 2005; Ishihara *et al.* 2009). If the dependence of C_{ϵ_θ} on Pr is known, one can obtain the dependence of R on Pr. For example, figure 2 of Buaria *et al.* (2021*a*)

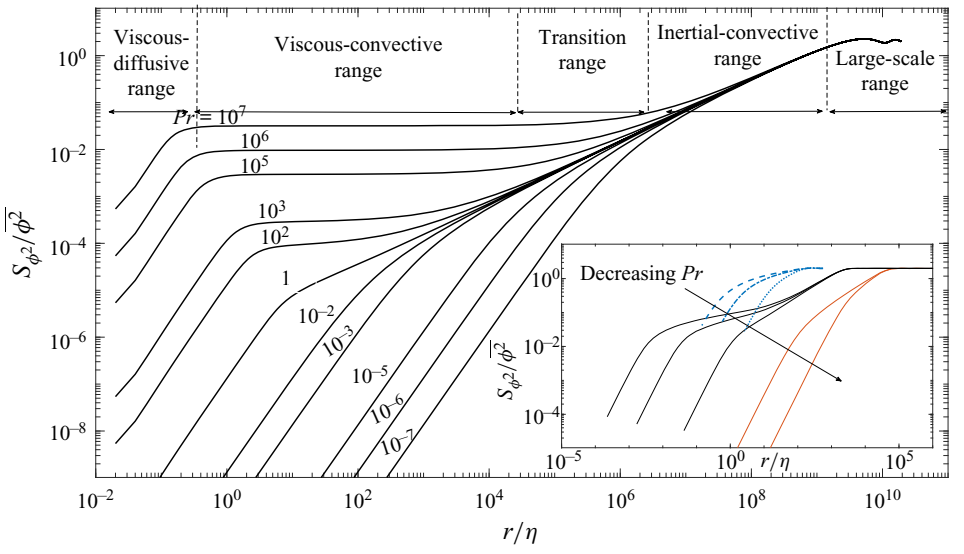

Figure 8. Effect of Pr on the distribution of $S_{\phi^2}/\overline{\phi^2}$ for $Re_\lambda = 1.15 \times 10^7$. The different subranges identified at the top refer to $Pr = 10^7$. Inset: EDQNM calculations for $Re_\lambda = 1000$ (black line) and $Re_\lambda = 20\,000$ (red line), $Pr = 10^5$, 10^3, 1, 10^{-3} and 10^{-5} (Briard & Gomez 2016). Blue lines: DNS (Buaria *et al.* 2021*b*), $Re_\lambda = 140$, $Pr = 512$ (dashed line), 32 (dot-dashed line) and 1 (dotted line).

shows that $C_{\epsilon\theta}$ varies like $1/\log Pr$ when $Re_\lambda = 140$ and Pr varies from 1 to 512 leading to $R \sim \log Pr$. Finally a few words are warranted regarding the calculations at very large values of Re_λ (e.g. $O(10^7)$) and Pr (e.g. $O(10^7)$). For such values of Re_λ, one expects the flow to be hypersonic and is unlikely to be observed in the laboratory or in the atmosphere. The results shown in figures 7 and 8 for very large Re_λ and Pr should be considered qualitative if not speculative.

6. Conclusions

We have solved numerically the linearly forced transport equation (1.1) for $\overline{(\delta\phi)^2}$, the second-order scalar function, using a closure model for $-\overline{(\delta u)(\delta\phi)^2}$, the third-order mixed velocity–scalar structure function. The closure, which exploits the analogy between the turbulent kinetic energy and passive scalar variance fields when $Pr = 1$, is based on a gradient-type hypothesis with an eddy-viscosity model proposed by Djenidi & Antonia (2021) for the third-order velocity structure function $\overline{(\delta u)^3}$. Further, a linear 'forcing' (4.2), similar to that introduced by Lundgren (2003) for the transport equation of $(\overline{(\delta u)^2})$, replaces the integral term in (1.1) in order to mimic steady-state HIT.

The calculated distributions of $\overline{(\delta\phi)^2}$ are tested against data reported in the literature and based on measurements and numerical simulations for $Pr = 0.7$ and 1. The agreement between the present calculations and published experimental and numerical data is very good lending confidence to the model (2.5) for closing the transport equation (1.1). However, the agreement deteriorates when Pr differs significantly from 1. Yet, the calculations reproduce the effect expected when Pr is varied. For example, as Pr increases, a range of scales emerges between the viscous–diffusive range and ICR, where $\overline{(\delta\phi)^2}$ remains constant. This range corresponds to the k^{-1} spectral range in

the three-dimensional scalar spectrum, but differs from that predicted by Batchelor (1959). Also when Pr decreases below 1, the calculation captures the expansion of the inertial–diffusive range to the detriment of the ICR.

Acknowledgements. We thank A. Briard for providing us with his EDQNM data. We also thank the reviewers for their constructive comments.

Funding. S.L.T. wishes to acknowledge support given to him from NSFC through grants 11702074 and 91952109 and from the Research Grants Council of Shenzhen Government through grant RCYX20210706092046085.

Declaration of interest. The authors report no conflict of interest.

Author ORCIDs.
L. Djenidi https://orcid.org/0000-0001-8614-3595;
S.L. Tang https://orcid.org/0000-0001-6379-8505.

References

Abe, H., Antonia, R.A. & Kawamura, H. 2009 Correlation between small-scale velocity and scalar fluctuations in a turbulent channel flow. *J. Fluid Mech.* **627**, 1–32.

Antonia, R.A., Abe, H. & Kawamura, H. 2009 Analogy between velocity and scalar fields in a turbulent channel flow. *J. Fluid Mech.* **628**, 241–268.

Antonia, R.A. & Orlandi, P. 2002 Dependence of the second-order scalar structure function on the Schmidt number. *Phys. Fluids* **14** (4), 1552–1554.

Antonia, R.A., Zhu, Y., Anselmet, F. & Ould-Rouis, M. 1996 Comparison between the sum of second-order velocity structure functions and the second-order temperature structure function. *Phys. Fluids* **8** (11), 3105–3111.

Batchelor, G.K. 1959 Small-scale variation of convected quantities like temperature in turbulent fluid part 1. General discussion and the case of small conductivity. *J. Fluid Mech.* **5** (1), 113–133.

Bogucki, D., Domaradzki, J.A. & Yeung, P.K. 1997 Direct numerical simulations of passive scalars with $Pr > 1$ advected by turbulent flow. *J. Fluid Mech.* **343**, 111–130.

Borgas, M.S., Sawford, B.L., Xu, S., Donzis, D.A. & Yeung, P.K. 2004 High Schmidt number scalars in turbulence: structure functions and Lagrangian theory. *Phys. Fluids* **16** (11), 3888–3899.

Briard, A. & Gomez, T. 2015 Passive scalar convective-diffusive subrange for low Prandtl numbers in isotropic turbulence. *Phys. Rev.* E **91** (1), 011001.

Briard, A. & Gomez, T. 2016 Mixed-derivative skewness for high Prandtl and Reynolds numbers in homogeneous isotropic turbulence. *Phys. Fluids* **28** (8), 081703.

Briard, A. & Gomez, T. 2017*a* Dynamics of helicity in homogeneous skew-isotropic turbulence. *J. Fluid Mech.* **821**, 539–581.

Briard, A. & Gomez, T. 2017*b* Prandtl number effects in decaying homogeneous isotropic turbulence with a mean scalar gradient. *J. Turbul.* **18** (5), 418–442.

Buaria, D., Clay, M.P., Sreenivasan, K.R. & Yeung, P.K. 2021*a* Turbulence is an ineffective mixer when Schmidt numbers are large. *Phys. Rev. Lett.* **126** (7), 074501.

Buaria, D., Clay, M.P., Sreenivasan, K.R. & Yeung, P.K. 2021*b* Small-scale isotropy and ramp-cliff structures in scalar turbulence. *Phys. Rev. Lett.* **126** (3), 034504.

Burattini, P., Antonia, R.A. & Danaila, L. 2005 Similarity in the far field of a turbulent round jet. *Phys. Fluids* **17**, 025101–025115.

Corrsin, S. 1951 On the spectrum of isotropic temperature fluctuations in an isotropic turbulence. *J. Appl. Phys.* **22** (4), 469–473.

Danaila, L., Anselmet, F., Zhou, T. & Antonia, R.A. 1999 A generalization of Yaglom's equation which accounts for the large-scale forcing in heated decaying turbulence. *J. Fluid Mech.* **391**, 359–372.

Danaila, L., Antonia, R.A. & Burattini, P. 2012 Comparison between kinetic energy and passive scalar energy transfer in locally homogeneous isotropic turbulence. *Phys.* D*: Nonlinear Phenom.* **241** (3), 224–231.

Djenidi, L. & Antonia, R.A. 2020 Assessment of large-scale forcing in isotropic turbulence using a closed Kármán–Howarth equation. *Phys. Fluids* **32** (5), 055104.

Djenidi, L. & Antonia, R.A. 2021 Modelling the third-order velocity structure function in the scaling range at finite Reynolds numbers. *J. Maths Phys.* **62** (3), 083102.

DJENIDI, L. & ANTONIA, R.A. 2022 Karmán-Howarth solutions of homogeneous isotropic turbulence. *J. Fluid Mech.* **932**, A30.

DJENIDI, L., ANTONIA, R.A. & DANAILA, L. 2017 Self-preservation relation to the Kolmogorov similarity hypotheses. *Phys. Rev. Fluids* **2** (5), 054606.

DONZIS, D.A., SREENIVASAN, K.R. & YEUNG, P.K. 2005 Scalar dissipation rate and dissipative anomaly in isotropic turbulence. *J. Fluid Mech.* **532**, 199–216.

FULACHIER, L. & ANTONIA, R.A. 1984 Spectral analogy between temperature and velocity fluctuations in several turbulent flows. *Intl J. Heat Mass Transfer* **27** (7), 987–997.

GAUDING, M., DANAILA, L. & VAREA, E. 2017 High-order structure functions for passive scalar fed by a mean gradient. *Intl J. Heat Fluid Flow* **67**, 86–93.

GOTOH, T. & WATANABE, T. 2015 Power and nonpower laws of passive scalar moments convected by isotropic turbulence. *Phys. Rev Lett.* **115** (11), 114502.

HANJALIĆ, K. 2002 One-point closure models for buoyancy-driven turbulent flows. *Annu. Rev. Fluid Mech.* **34** (1), 321–347.

ISHIHARA, T., GOTOH, T. & KANEDA, Y. 2009 Study of high-Reynolds number isotropic turbulence by direct numerical simulation. *Annu. Rev. Fluid Mech.* **41**, 165–180.

JIANG, T.L. & O'BRIEN, E.E. 1991 Simulation of scalar mixing by stationary isotropic turbulence. *Phys. Fluids* A*: Fluid Dyn.* **3** (6), 1612–1624.

KÁRMÁN, T.V. & HOWARTH, L. 1938 On the statistical theory of isotropic turbulence. *Proc. R. Soc. Lond.* A **164**, 192–215.

LUNDGREN, T.S. 2003 Linearly forced isotropic turbulence. *Annu. Rev. Briefs Center Turbul. Res.* **ADP014826**, 461–473.

MONIN, A.S. & YAGLOM, A.M. 1975 *Statistical Fluid Mechanics: Mechanics of Turbulence, Vol. II (Republication, 2007)*. Dover Publications.

MYDLARSKI, L. & WARHAFT, Z. 1998 Passive scalar statistics in high-Péclet-number grid turbulence. *J. Fluid Mech.* **358**, 135–175.

OBOUKHOV, A.M. 1949 Structure of the temperature field in turbulent flows. *Isv. Geogr. Geophys. Ser.* **13**, 58–69.

RISTORCELLI, J.R. 2006 Passive scalar mixing: analytic study of time scale ratio, variance, and mix rate. *Phys. Fluids* **18** (7), 075101.

SHETE, K.P. & DE BRUYN KOPS, S.M. 2020 Area of scalar isosurfaces in homogeneous isotropic turbulence as a function of Reynolds and Schmidt numbers. *J. Fluid Mech.* **883**, A38.

SREENIVASAN, K.R. 1995 On the universality of the Kolmogorov constant. *Phys. Fluids* **7** (11), 2778–2784.

SREENIVASAN, K.R. 1996 The passive scalar spectrum and the Obukhov–Corrsin constant. *Phys. Fluids* **8** (1), 189–196.

TENNEKES, H. & LUMLEY, J.L. 1972 *A First Course in Turbulence*. MIT Press.

WATANABE, T. & GOTOH, T. 2004 Statistics of a passive scalar in homogeneous turbulence. *New J. Phys.* **6** (1), 40.

YAGLOM, A.M. 1949 On the local structure of a temperature field in a turbulent flow. *Dokl. Akad. Nauk SSSR* **69** (6), 743–746.

YEH, T.T. & ATTA, C.W. 1973 Spectral transfer of scalar and velocity fields in heated-grid turbulence. *J. Fluid Mech.* **58** (2), 233–261.

YEUNG, P.K. & SREENIVASAN, K.R. 2014 Direct numerical simulation of turbulent mixing at very low Schmidt number with a uniform mean gradient. *Phys. Fluids* **26** (1), 015107.

YEUNG, P.K., XU, S., DONZIS, D.A. & SREENIVASAN, K.R. 2004 Simulations of three-dimensional turbulent mixing for Schmidt numbers of the order 1000. *Flow Turbul. Combust.* **72** (2), 333–347.

YEUNG, P.K., XU, S. & SREENIVASAN, K.R. 2002 Schmidt number effects on turbulent transport with uniform mean scalar gradient. *Phys. Fluids* **14** (12), 4178–4191.